Spectral Energetics of the General Circulation and Time Spectra of Transient Waves during the FGGE Year*

ERNEST C. KUNG

Department of Atmospheric Science, University of Missouri—Columbia, Columbia, Missouri

(Manuscript received 18 March 1987, in final form 7 August 1987)

ABSTRACT

The spectral energetics of the general circulation are presented for the entire FGGE year based on the GFDL analyses of FGGE observations. The global energy balance and those of the Northern and Southern hemispheres show a reasonable agreement. However, examining the energy flow in the wavenumber domain reveals a marked contrast between the two hemispheres in both energy and energy transformations. The annual variations of energy variables are large, and there are also pronounced differences of seasonal characteristics between the two hemispheres.

With the one-year time series of energy variables, time spectra of transient waves are examined at 500 and 100 mb in order to evaluate their contribution to the time-averaged kinetic energy and baroclinic conversion. Characteristic distributions of power spectra for kinetic energy and available potential energy are described for the Northern and Southern hemispheres. In cyclone-scale disturbances almost the entire baroclinic conversion is supported by transient waves. There are pronounced contrasts between the Northern and Southern hemispheres in the conversion cospectra at various zonal wavenumbers.

1. Introduction

The availability of global gridded data from the First GARP (Global Atmospheric Research Program) Global Experiment (FGGE) presents an opportunity for a comprehensive energetics diagnosis of the general circulation. The global circulation models and techniques employed in data assimilation may influence the dataset produced. Yet energetics comparisons of the assimilated data and parallel simulations indicate that the former clearly represent the observed fields of the general circulation rather than the model atmosphere (e.g., Kung and Baker, 1986a,b). Further, despite differences exhibited by various versions of FGGE datasets, we may expect a reasonable agreement among them in representing the observed circulation of the atmosphere (see Chen and Lee, 1985; Lorenc and Swinbank, 1984; Rosen and Salstein, 1980).

A number of spectral energetics studies with the FGGE data are available. Kung and Tanaka (1983, 1984) described the gross spectral characteristics of the global energetics, including the energy flow in the wavenumber domain, for the special observing periods (SOP-1 and SOP-2). The winter and summer spectral energetics of the Northern and Southern hemispheres were examined by Chen and Lee (1985) with various sets of level IIIb data. Lambert (1986) studied the nonlinear exchanges of eddy kinetic energy in the Southern Hemisphere for January and July. In an attempt to examine the simulation capability of global circulation models, Kung and Baker (1986a,b) conducted comparative energetics studies for the observed and simulated global circulation of SOP-1 and SOP-2, and for the Northern Hemisphere circulation during winter blocking episodes. Further, to describe energy properties of Rossby and gravity modes and associated transformations, a three-dimensional normal mode energetics scheme was developed and applied to observations and to simulations by Tanaka et al. (1986).

Most of the FGGE energetics studies, however, have been performed with data from limited time periods. One exception is the study by Arpe et al. (1986) which included the European Centre for Medium Range Weather Forecasts (ECMWF) FGGE level IIIb analyses for the entire FGGE year. Nevertheless, this energetics analysis was presented in the zonal mean-eddy partitioning format without a breakdown into wavenumber components. It is then very desirable to examine the energetics characteristics of the global circulation through the entire FGGE year in light of the earlier FGGE studies. The FGGE year covers a one-year period from 1 December 1978 to 30 November 1979. Although the dataset for a one-year period does not allow the study of interannual variations, a gross

* Missouri Agricultural Experiment Station Contribution No. 10287.

Corresponding author address: Prof. Ernest C. Kung, Dept. of Atmospheric Science, University of Missouri—Columbia, 701 Hitt Street, Columbia, Missouri 65211.

budget and time series analysis for the entire FGGE year will provide baseline information for future diagnoses of the general circulation. In this study the annual mean global energy balance and the contrast between the Northern and Southern hemispheres are presented in the wavenumber domain using the Geophysical Fluid Dynamics Laboratory (GFDL) FGGE level IIIb analyses. Time variations of the energetics variables are then examined in terms of monthly variations and power spectral analysis of the time series during the FGGE year.

We use the GFDL version of the FGGE dataset because only the ECMWF and GFDL analyses are available through the entire FGGE year. Currently both datasets are in the process of being reanalyzed by ECMWF and GFDL. The GFDL analyses were chosen over the ECMWF analyses because the multivariate optimum interpolation scheme used in the ECMWF analyses suppressed the divergent field of the wind, and, in turn, the vertical motion field generated by the kinematic method (see Chen and Lee, 1985). Comparative spectral energetics analyses by Chen and Lee (1985) and Kung and Tanaka (1983) both indicate that the ECMWF analyses exhibit the lowest energy levels and weakest energy transformations among the FGGE datasets. Kung and Tanaka further show that the ageostrophic kinetic energy production of the ECMWF analyses is very weak in the upper troposphere. It is important, however, to point out that the GFDL analyses also seem to possess some major problems. Comprehensive comparative statistics by Rosen et al. (1985) reveal an excessively strong Hadley circulation in the GFDL analyses (also see Kung and Tanaka, 1983). This makes direct computations of energy variables with the zonal mean vertical motion field difficult. Rosen et al. also point out that continuous data insertion used by GFDL tends to excite excessive gravity noise. According to Miyakoda et al. (1982) the GFDL global optimum interpolation in the final stage of the forecast/analysis cycle may cause a dynamic imbalance in the dataset. The intercomparisons of various datasets, however, are readily available in the literature, and the results presented with the GFDL analyses will be useful in understanding the energetics characteristics of the general circulation.

The energy equations in the one-dimensional zonal wavenumber domain, as used in this study, were originally proposed by Saltzman (1957, 1970), and they have proven their usefulness in the energetics description of the general circulation. The scheme, however, may not always allow a simple interpretation of energetics budgets (e.g., McIntyre, 1980; Plumb, 1983). For the study of specific systems or mechanisms in the general circulation, it is often desirable to supplement the zonal spectral energetics with a local energy budget or with an additional energetics scheme such as a three-dimensional normal mode scheme (Tanaka et al., 1986). However, the spectral energetics in the zonal wavenumber domain offers the most convenient energetics description of the general circulation, to which other specific schemes can be easily related.

2. Energy equations and scheme of analysis

Since the details of the analysis scheme are available in our preceding reports (Kung and Baker, 1986a; Kung and Tanaka, 1983, 1984), only an abbreviated description of the energy equations and their evaluation are provided here. Table 1 lists symbols, definitions, and variables used in this paper.

The equations of kinetic energy and available potential energy in the zonal wavenumber domain may be written, after Saltzman (1957, 1970), as

$$\frac{\partial K(0)}{\partial t} = \sum_{n=1}^{N} M(n) + C(0) - D(0) \tag{1}$$

$$\frac{\partial K(n)}{\partial t} = -M(n) + L(n) + C(n) - D(n), \quad n \neq 0 \tag{2}$$

TABLE 1. Symbols, definitions, and variables.

t	time
$\mathbf{V}$	horizontal wind vector
m	mass of the atmosphere
ϕ	geopotential
∇	horizontal del operator along an isobaric surface
U	complex-valued coefficient of u-component of wind
V	complex-valued coefficient of v-component of wind
B	complex-valued coefficient of temperature
Ω	complex-valued coefficient of vertical velocity
q_M	annual mean component of an arbitrary function q
q_A	annual cycle of q
q_T	transient component of q
n	zonal wavenumber
N	maximum zonal wavenumber
$K(n)$	kinetic energy at wavenumber n
$P(n)$	available potential energy at wavenumber n
$M(n)$	transfer of $K(n)$ to $K(0)$ where $n \neq 0$
$L(n)$	transfer of eddy kinetic energy from all other wavenumbers to $K(n)$ where $n \neq 0$
$C(n)$	conversion of $P(n)$ to $K(n)$
$R(n)$	transfer of $P(0)$ to $P(n)$ where $n \neq 0$
$S(n)$	transfer of eddy available potential energy from all other wavenumbers to $P(n)$ where $n \neq 0$
$D(n)$	dissipation of $K(n)$
$G(n)$	generation of $K(n)$
K_M	zonal mean kinetic energy
K_E	zonal eddy kinetic energy
P_M	zonal mean available potential energy
P_E	zonal eddy available potential energy
$M(K_E, K_M)$	conversion from K_E to K_M
$C(P_E, K_E)$	conversion from P_E to K_E
$R(P_M, P_E)$	conversion of P_M to P_E
$D(K_E)$	dissipation of K_E
$G(P_E)$	generation of P_E
$-\mathbf{V}\cdot\nabla\phi$	production of kinetic energy by cross-isobaric motion

$$\frac{\partial P(0)}{\partial t} = -\sum_{n=1}^{N} R(n) - C(0) + G(0) \tag{3}$$

$$\frac{\partial P(n)}{\partial t} = R(n) + S(n) - C(n) + G(n), \quad n \neq 0. \tag{4}$$

The equations of eddy kinetic energy and available potential energy may be obtained by summing (2) and (4) from $n = 1$ to the maximum wavenumber N:

$$\frac{\partial K_E}{\partial t} = -M(K_E, K_M) + C(P_E, K_E) - D(K_E) \tag{5}$$

$$\frac{\partial P_E}{\partial t} = R(P_M, P_E) - C(P_E, K_E) + G(P_E). \tag{6}$$

Equations (1)–(6) state the balance requirement over the total mass of the atmosphere. When the equations are applied over the Northern and Southern hemispheres, an equatorial wall is assumed at the boundary of both hemispheres to avoid computing the cross-equatorial flux of potential energy. Our computation with the GFDL and other datasets indicates that the total cross-equatorial flux of kinetic energy is 0.02–0.03 W m^{-2} in winter and summer. However, the potential energy fluxes by eddies and zonal mean motion across the equator are, respectively, on the order of 0.1 W m^{-2} and 1–2 W m^{-2}. The direction of flux is from the summer to winter hemisphere, which parallels the movement of the summer hemisphere Hadley cell into the winter hemisphere. However, the magnitude of potential energy flux, particularly that of the zonal mean component, is erroneously large in view of the global energy balance (see Fig. 1). The spuriously large transport is apparently caused by large values of potential energy in the higher levels of the atmosphere, which grossly amplifies the errors involved in observation and data assimilation. The placement of an equatorial wall is thus necessary, although it leaves out the question of the real cross-equatorial transport. Comparison of the gross energy budgets of the Northern and Southern hemispheres with the global budget, as shown in Fig. 1, seems to indicate that an equatorial wall is acceptable in computing the hemispheric budgets.

As pointed out by Chen and Lee (1985), Kung and Baker (1986a), and Kung and Tanaka (1983), uncertainty in the magnitude of the zonal mean vertical motion in various FGGE datasets seems to overly influence the computed values of the zonal mean conversion $C(0)$. According to Chen and Lee, the computed value of $C(0)$ during SOP-1 ranges from -0.66 W m^{-2} for the ECMWF analyses to 2.23 W m^{-2} for the GFDL analyses, with 0.01 W m^{-2} for the Goddard Laboratory for Atmospheres (GLA) analyses. Apparently, the GFDL analyses overestimate $C(0)$ for the very strong Hadley cells (see Rosen et al., 1985). Thus, to minimize the effect of errors in the zonal mean vertical motion, the relationship

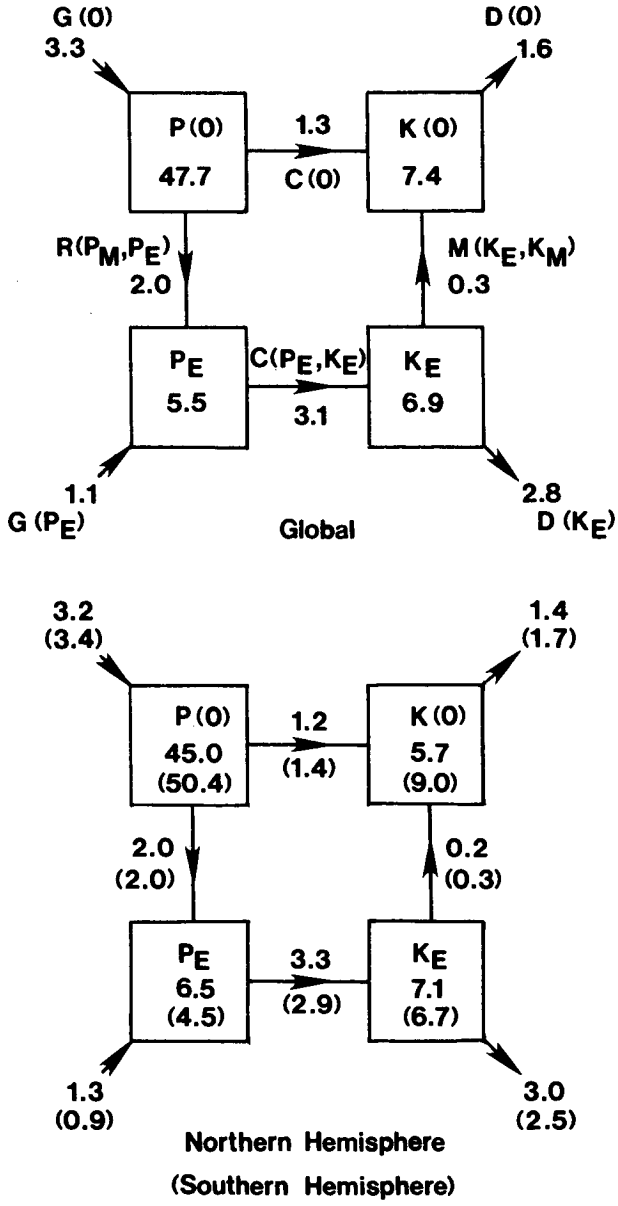

FIG. 1. Global and hemispheric mean energy balances during the FGGE year. Energy is in units of 10^5 J m^{-2} and transformation in W m^{-2}.

$$C(0) = -\int_m \mathbf{V} \cdot \nabla\phi dm - \sum_{n=1}^{N} C(n) \tag{7}$$

is used to remove the direct dependence of $C(0)$ on the zonal mean field of vertical motion. It has been shown that the computation of $-\mathbf{V} \cdot \nabla\phi$ with a dataset without a geostrophic constraint, such as the GFDL analyses, yields reasonable values of ageostrophic production of kinetic energy (e.g., Holopainen and Eerola, 1979; Kung, 1977; Kung and Tanaka, 1983). This is not the case in a dataset with a geostrophic constraint such as the ECMWF analyses (see Kung and Tanaka, 1983).

To avoid the problem of $-\mathbf{V}\cdot\nabla\phi$ computations associated with the lower boundary, the surface value of $-\mathbf{V}\cdot\nabla\phi$ is obtained from the surface wind vector and the $\nabla\phi$ value at 1000 mb, setting the lower boundary of vertical integration at surface pressure.

The eddy variables in (5) and (6) are obtained as spectral sums over wavenumbers n = 1–30, and the dissipation terms of kinetic energy and generation terms of available potential energy in (1)–(6) are obtained as residual terms to balance the respective equations. For the wavenumber interactions $L(n)$ and $S(n)$, however, no specific attempt is made to adjust the computational results to achieve a balance among wavenumbers. The energy variables are presented for the mass of the atmosphere from the surface to 50 mb unless stated otherwise.

The feasibility of examining large-scale turbulence in frequency–wavenumber space is presented by Kao (1968) in his comprehensive formulation of the problem. In this study, a power spectral analysis of the time series is applied to the transient components of energy variables in the Northern and Southern hemispheres. The complex-valued coefficient $U(t)$ of the u-component of wind for a zonal wavenumber n is partitioned into

$$U(t) = U_M + U_A(t) + U_T(t) \tag{8}$$

where U_M is the annual mean, U_A the annual cycle, and U_T the transient component. After subtracting U_M from $U(t)$, the first harmonic of the one-year time series is taken as the annual variation $U_A(t)$, and the residual in (8) is considered to be the transient component $U_T(t)$ without the annual variation. The power spectra of $U_T(t)$ are then computed at 500 and 100 mb for each wavenumber as aperiodic functions of frequency. The complex-valued coefficient $V(t)$ of the v-component of wind is processed in the same way, and the sum of the power spectra of $U_T(t)$ and $V_T(t)$ at wavenumber n gives the spectra of kinetic energy $K(n)$ of the transient waves. The spectra of available potential energy $P(n)$ of transient waves are given by the power spectra of the transient component of the complex-valued coefficient $B_T(t)$ of temperature with global mean static stability parameters obtained from the annual mean temperature at 500 and 100 mb. In the case of $n = 0$, the zonal average of the deviation of temperature from the hemispherical mean is used in lieu of $B_T(t)$. In a similar manner, the baroclinic conversion $C(n)$ of transient waves is examined using cospectra of transient components of complex-valued coefficients $B_T(t)$ of temperature and $\Omega_T(t)$ of vertical velocity. All the complex-valued coefficients used in the time series are averaged for each hemisphere.

The original level IIIb GFDL analyses on a 1.87° × 1.87° latitude–longitude grid from 1 December 1978 to 30 November 1979 were interpolated to a 4° × 5° grid from 90°S to 90°N and from 0° to 355°E as described by Kung and Tanaka (1983). The data include twice-daily values at 0000 and 1200 UTC for geopotential height, temperature, horizontal wind, and vertical velocity at 1000, 850, 700, 500, 400, 300, 250, 200, 150, 100 and 50 mb. All energy variables are computed at each of the twice-daily analysis times. However, the computed values are averaged for each day to eliminate diurnal variations from the time series.

3. Global spectral energy balance and hemispheric contrasts

The gross energy balance of the general circulation during the FGGE year is summarized in Fig. 1 in Lorenz' (1955) box diagrams for the global mean and for the Northern and Southern hemispheres. The global mean energy balance for the entire FGGE year is very close to the average of SOP-1 and SOP-2 obtained by Kung and Tanaka (1983) with the same dataset. There is an overall agreement on the direction of the energy flow with the previous observational estimates of the energy cycle (e.g., Oort and Peixoto, 1983; Newell et al., 1970; Saltzman, 1970; Wiin-Nielsen, 1968). However, there are considerable numerical variations between the present FGGE estimate and previous estimates. Most of the discrepancies may be attributable to the fact that the data coverage of the earlier estimates was mainly restricted to the middle latitudes of the Northern Hemisphere. According to the global energy balance in Fig. 1, the intensity of the general circulation as measured by $G(0) + G(P_E)$, $C(0) + C(P_E, K_E)$, or $D(0) + D(K_E)$ is 4.4 W m^{-2}, or 1.3% of one-fourth of the solar constant.

As discussed in section 2, the estimate of the zonal mean conversion $C(0)$ is uncertain in various analyses. Thus caution must be exercised in adopting a computed value in order to balance the global or hemispheric budget. Rosen et al. (1985) computed this term independently for the Northern Hemisphere during January and June 1979 with the GFDL and traditional station-based analyses, using the monthly mean fields of the zonal mean u- and v-components of wind. Their winter and summer values of 1.72 and 0.06 W m^{-2} yield an average of 0.89 W m^{-2} with the GFDL data, and an average of 0.54 W m^{-2} with the station-based data of 0.76 and 0.31 W m^{-2}. Considering that estimates by Rosen et al. are based on the monthly mean fields of the circulation, their estimates of $C(0)$ compare favorably with our estimate of $C(0)$ = 1.2 W m^{-2} for the Northern Hemisphere (Fig. 1). Likewise, the estimates of $R(P_M, P_E)$ and $M(K_E, K_M)$ by Rosen et al. also agree favorably with ours.

Chen and Lee's (1985) energy budgets for the FGGE winter in the Northern Hemisphere show negative values for $C(0)$ with the ECMWF analyses. This corresponds with Kung and Tanaka's (1983) estimate with the same dataset, reflecting the problems with the Hadley cells in the early version of the ECMWF anal-

yses. Chen and Lee's estimate of $M(K_E, K_M)$ with the GFDL analyses shows small negative values. The discrepancy of their estimate with ours and that of Rosen et al. (1985) cannot be resolved at present. The gross energy balance obtained by Arpe et al. (1986) from the ECMWF FGGE and operational analyses and ECMWF forecasts is basically similar to Kung and Tanaka's (1983) computed with the ECMWF analyses. The value of $C(0)$ is negative. The change of sign is also noted for $G(P_E)$ between the initialized analyses and 12 h forecasts, and between the hemispheres.

The energy flow in the box diagrams of Fig. 1 shows a similar basic pattern for both the Northern and Southern hemispheres as the global mean. The largest energy flow proceeds from $P(0)$ via P_E to K_E, and some K_E is further transformed to $K(0)$. Dissipation takes place in both K_E and $K(0)$. There is a direct generation of P_E, and the direct conversion between $P(0)$ and $K(0)$ is also appreciable. It is apparent, however, that both for kinetic energy and available potential energy the zonal mean components in the Southern Hemisphere are much larger than those in the Northern Hemisphere, and the eddy components in the former are smaller than those in the latter. The totals of zonal mean and eddy components are significantly larger in the Southern Hemisphere than in the Northern Hemisphere both for kinetic and available potential energy. These contrasts obviously reflect the stronger differential heating and more uniform topography of the Southern Hemisphere, which has a predominant water surface. However, the differences between hemispheres in energy transformations are not clear in the box diagrams, since the large differences in the wavenumber domain, as will be discussed later, disappear when summed up over all wavenumbers.

Figure 2 illustrates the annual mean energy flow for each wavenumber for $n = 0$–15. In the annual mean budget the contribution from $n = 15$–30 is negligible and is therefore omitted. Although the ultralong and large cyclone-scale waves contribute to the eddy generation $G(n)$, conversion $C(n)$, and dissipation $D(n)$ more significantly than the short synoptic waves, the contribution of the latter is by no means negligible. For the nonlinear wave–wave interactions $S(n)$ and $L(n)$ and wave–mean interaction $M(n)$, the contribution of short waves beyond $n = 7$ is small. It should be emphasized, however, that an energy flow pattern for a single observation time or that associated with a specific synoptic development may deviate markedly from the annual mean pattern. For example, Kung and Baker (1986b) illustrated that the wave–wave interaction of kinetic energy $L(6$–$10)$ during a period of blocking development in the Northern Hemisphere becomes several times larger than the annual mean value to support the amplification of the ultralong waves. Examination of the daily time series against the annual mean pattern reveals that $S(n)$, $L(n)$ and $M(n)$ from ultralong to short cyclone-scale waves are all active for individual observation times, although the daily significance of medium and short cyclone-scale waves is cancelled out in a long time mean. For $G(n)$, $R(n)$, $C(n)$ or $D(n)$, the daily spectral distribution patterns over all wave ranges are well preserved in the annual mean pattern. This may indicate that the wave–wave and wave–mean nonlinear interactions of kinetic energy, $L(n)$ and $M(n)$, and wave–wave nonlinear interaction of available potential energy $S(n)$ are more closely associated with the manifestations of synoptic disturbances, whereas other transformation processes are more closely associated with the maintenance of the basic patterns of the general circulation.

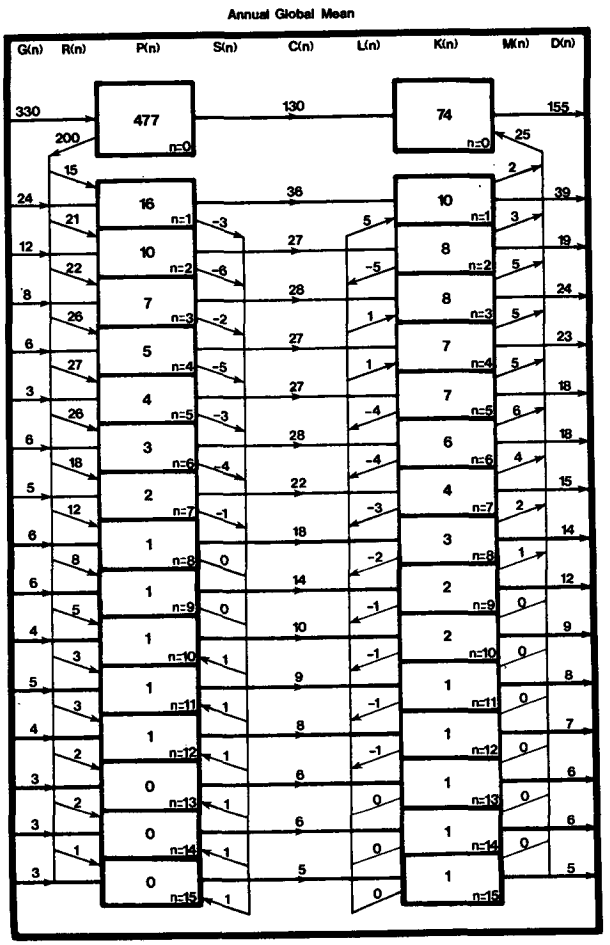

FIG. 2. Global energy flow diagram in the wavenumber domain during the FGGE year. Energy is in units of 10^4 J m^{-2} and transformation in 10^{-2} W m^{-2}.

The annual mean spectral distributions of $P(n)$ and $K(n)$ are compared between the Northern and Southern hemispheres in Fig. 3. The large $P(0)$ and $K(0)$ in the Southern Hemisphere (Fig. 1) apparently come at the expense of $P(n)$ and $K(n)$ of ultralong waves $n = 1$–3. The large land–sea contrast of the middle latitudes of the Northern Hemisphere leads to the dominance of ultralong waves in that portion of the atmosphere. The

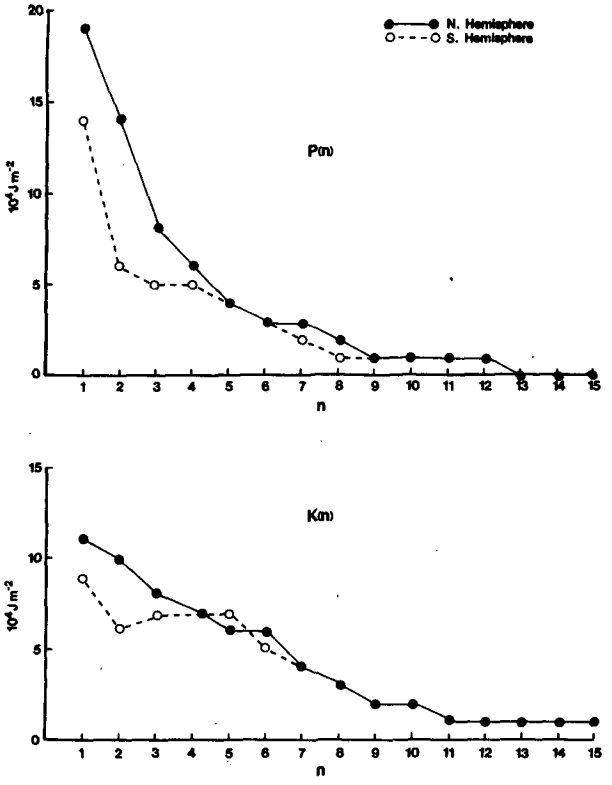

FIG. 3. Spectral distributions of $P(n)$ and $K(n)$ in the Northern and Southern hemispheres during the FGGE year.

contrast of the Northern and Southern hemispheres is particularly strong at $n = 2$.

As indicated in Figs. 4 and 5, the dominance of ultralong waves in the Northern Hemisphere over those in the Southern Hemisphere is supported by a large transfer of zonal available potential energy into $n = 2$–3, and subsequently large conversion of available potential energy to kinetic energy $C(2\text{–}3)$. In the Southern Hemisphere, the generation of available potential energy $G(1)$ and corresponding conversion $C(1)$ are large, but $P(1)$ and $K(1)$ are respectively depleted by wave–wave interactions $S(1)$ and $L(1)$ to shorter wavenumbers. In the Southern Hemisphere, the mean-wave transfer of available potential energy $R(n)$ is most active at $n = 4$–6, with corresponding large baroclinic conversion $C(4\text{–}6)$. However, both $P(n)$ and $K(n)$ are depleted by the wave–wave interactions $S(n)$ and $L(n)$ and also by wave–mean interaction $M(n)$ at this range. Consistently more active baroclinic conversion $C(n)$ is noted in the Northern Hemisphere in all waves beyond $n = 6$.

Chen and Lee (1985) presented spectral distributions of energy and transformations for the FGGE winter and summer separately for the Northern and Southern hemispheres. Their computed spectra with various FGGE datasets are qualitatively in agreement with our annual mean spectra. Lambert (1986) computed the eddy kinetic energy transformations of $n = 1$–10 for the Southern Hemisphere. Although his presentation covers only January and July of 1979, a qualitative agreement of his spectral distribution with ours and Chen and Lee's may be recognized.

4. Annual variations

Kung and Tanaka (1983, 1984) and Chen and Lee (1985) noted pronounced differences in energy levels and transformations in the Northern Hemisphere between SOP-1 and SOP-2. The differences, however, were much less in the Southern Hemisphere. This leads to a large seasonal contrast of the globally integrated energy budget which comes mostly from the Northern Hemisphere.

With the analysis data of the entire FGGE year, the annual hemispheric variations of $K(0)$ and $P(0)$ are shown in Figs. 6 and 7, and those of $K(n)$ and $P(n)$ in Fig. 8 for $n = 1$–4 over which the seasonal differences are most evident. Both the Northern and Southern hemispheres possess the highest level of energy in their respective winters and the lowest in the summer. The

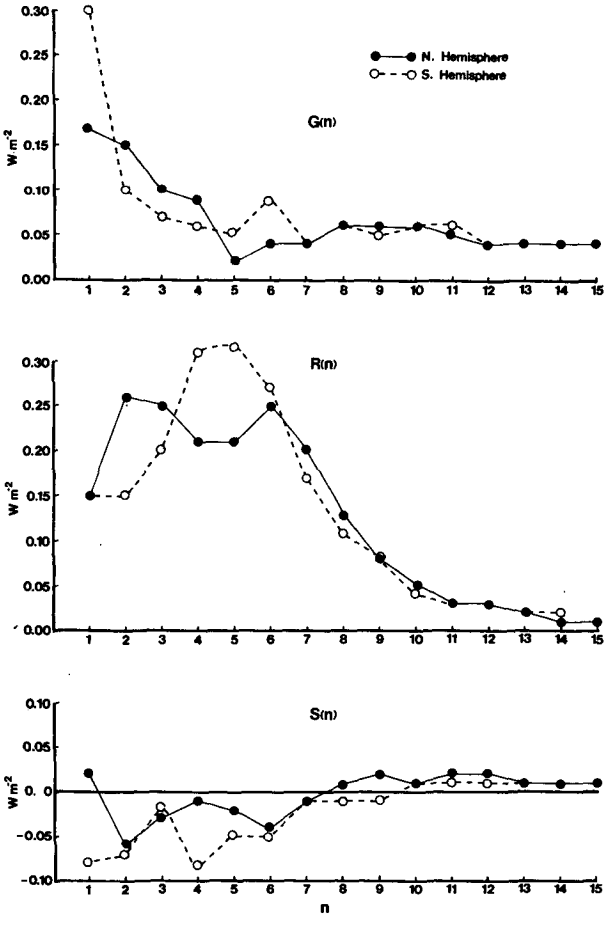

FIG. 4. As in Fig. 3 except for $G(n)$, $R(n)$ and $S(n)$.

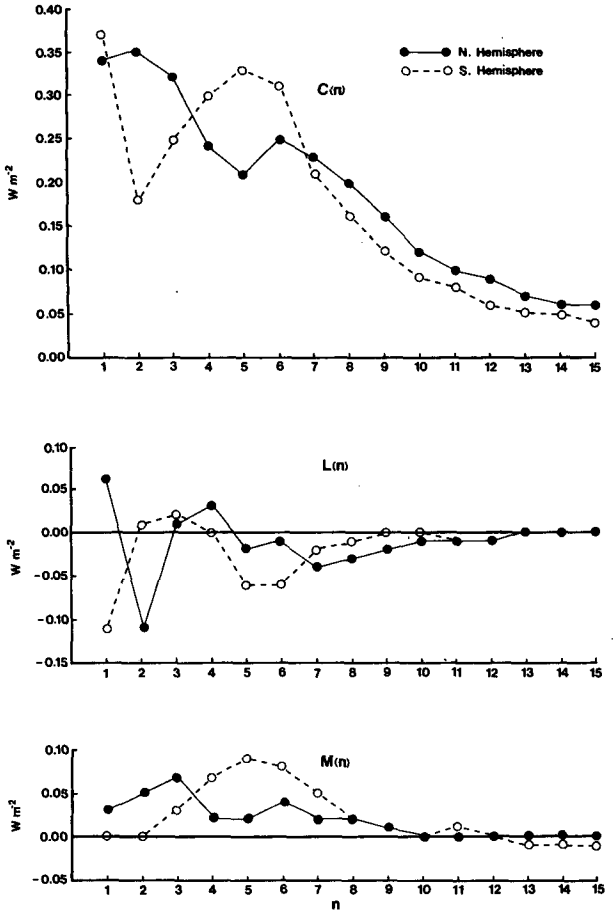

FIG. 5. As in Fig. 3 except for $C(n)$, $L(n)$ and $M(n)$.

spring transition into summer seems more rapid than the fall buildup into winter. The hemispheric differences in $K(0)$ and $P(0)$ are largest in the Northern summer (Southern winter) because of the very high Southern Hemisphere energy level and very low Northern Hemisphere energy. However, for $K(n)$ and $P(n)$ of n = 1–3, the hemispheric differences are more pronounced in the Northern winter (Southern summer) because of the amplified ultralong waves of the Northern Hemisphere in the winter. This is an obvious result of the Northern Hemisphere winter heating field in association with the topography and land–sea distribution. If the energy components are integrated over the globe and all wavenumbers, we may expect a global seasonal variation as presented by Arpe et al. (1986).

Annual variations of the baroclinic conversion $C(n)$ in the Northern and Southern hemispheres are contrasted in Fig. 9 for n = 1–7. It is interesting to note that in the Northern Hemisphere $C(1)$ has a primary maximum in August and a secondary maximum, which is much smaller, in January, although all other Northern Hemisphere conversions $C(n)$ have the maxima in the winter and the minima in the summer. The large Northern Hemisphere conversion by n = 1 in the summer is associated with the summer monsoon system in the subtropical latitudes, as indicated by Kung and Tanaka's (1984) SOP-2 latitudinal distribution of $C(1)$.

During the northern winter, the strong conversion by n = 2 dominates along with those by n = 3–4 in support of the amplified ultralong waves. Because of the dominance of $C(2)$ in the northern winter, $C(2)$ also shows the largest hemispheric difference among all waves in all seasons. From April to October, the hemispheric difference in $C(2)$ is very limited. For n = 3–6, however, the stronger $C(n)$ in the Southern Hemisphere becomes noticeable during the Northern summer (Southern winter) with the maximum hemispheric difference at n = 5. From n = 7 and beyond, the hemispheric difference becomes less distinctive and almost indistinguishable in the short-wave range.

This study is based on one-year data during the FGGE and thus the problem of interannual variations is beyond the scope of the present investigation. Arpe et al. (1986) used various ECMWF data from 1979 to 1985 to compute energetics in zonal mean and eddy partitioning. The standard deviations of interannual variations in energy levels are only 1–2% of the multiannual averages. Transformations, with the exception of $C(0)$ and $G(P_E)$, also show interannual variations of less than 10%, and mainly within 5%. If this is an indication of the interannual variation of energetics in the general circulation, the energetics characteristics presented in this study should not be subject to large interannual variations.

5. Time spectra of transient waves

After subtracting the annual mean and annual variation from the one-year time series, as illustrated with $U(t)$ in (8), the residual time series may be treated as describing transient waves. The residual daily time series of the one-year period allows us to compute stable power spectra for periods of 2–128 days. Figures 10 and 11 show the time spectra of $K(n)$ and $P(n)$ of transient waves for n = 0, 1, 2 and 5 at 500 and 100 mb from 4–128 day periods. Because the annual variation, the largest component of the time variation (see Figs. 6 and 7), has been filtered out from the original time series, the power spectra obtained are appropriate to examine the transient character of the zonal waves. The variance associated with periods between 128 days and 1 year is confirmed in computations to be negligible.

The time spectra of $K(0)$, $K(1)$, and $K(2)$ indicate a gradual increase of energy from the shortest period to 30–60 days and then a sudden drop of energy density beyond that. Both the Northern and Southern hemispheres show a similar trend, but for $K(0)$ the energy peak is reached earlier in the Northern Hemisphere. At 100 mb the sharp increase of energy density for

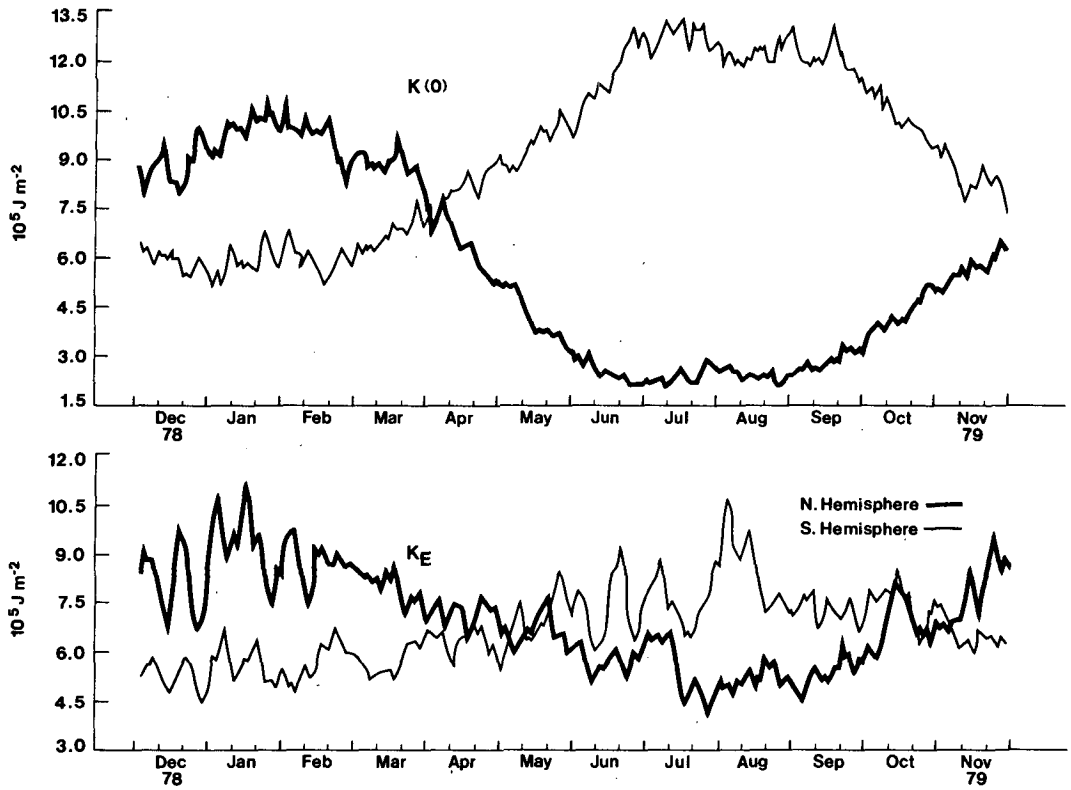

FIG. 6. Daily time variations of $K(0)$ and K_E in the Northern and Southern hemispheres during the FGGE year.

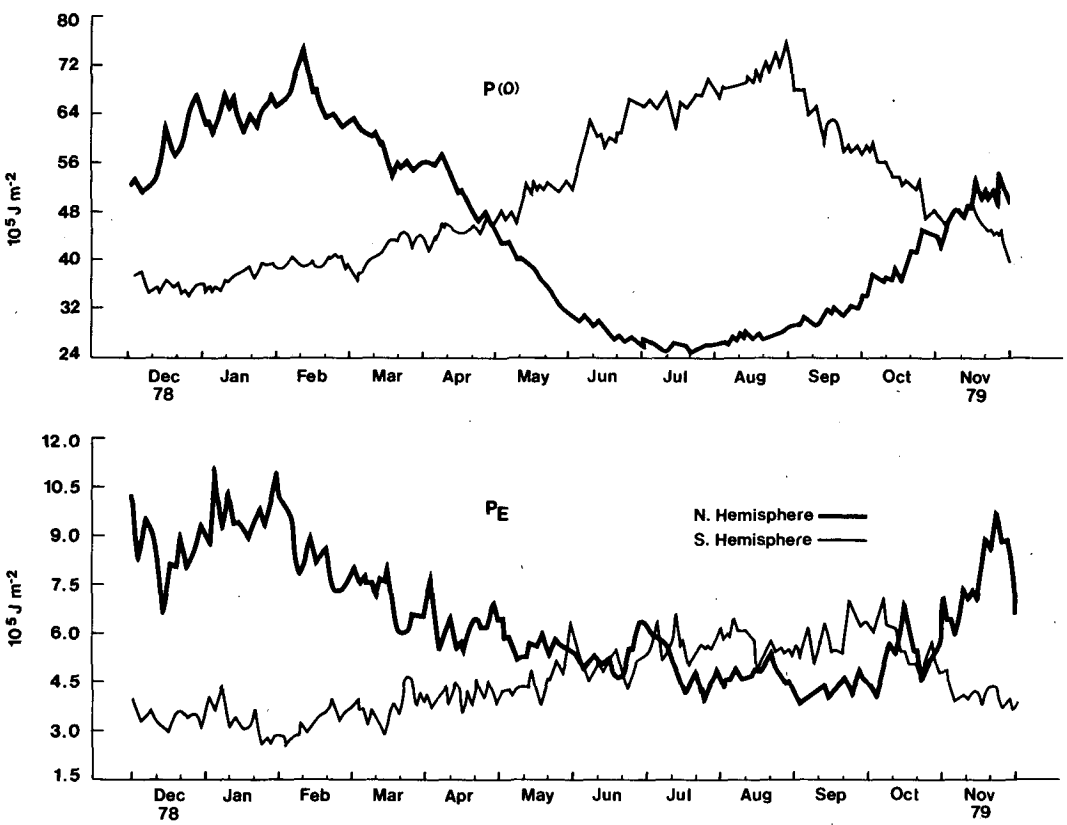

FIG. 7. As in Fig. 6 except for $P(0)$ and P_E.

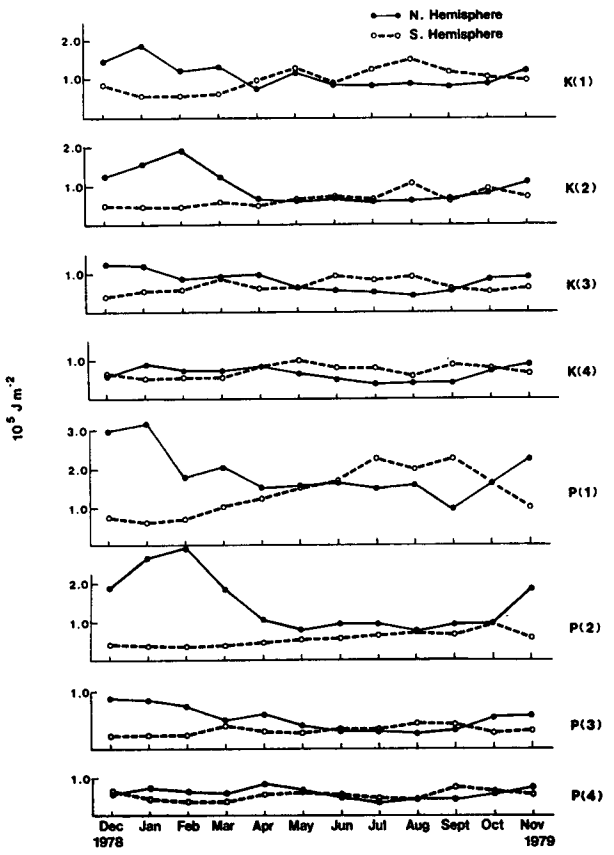

FIG. 8. Monthly time variations of $K(n)$ and $P(n)$ for n = 1–4 in the Northern and Southern hemispheres during the FGGE year.

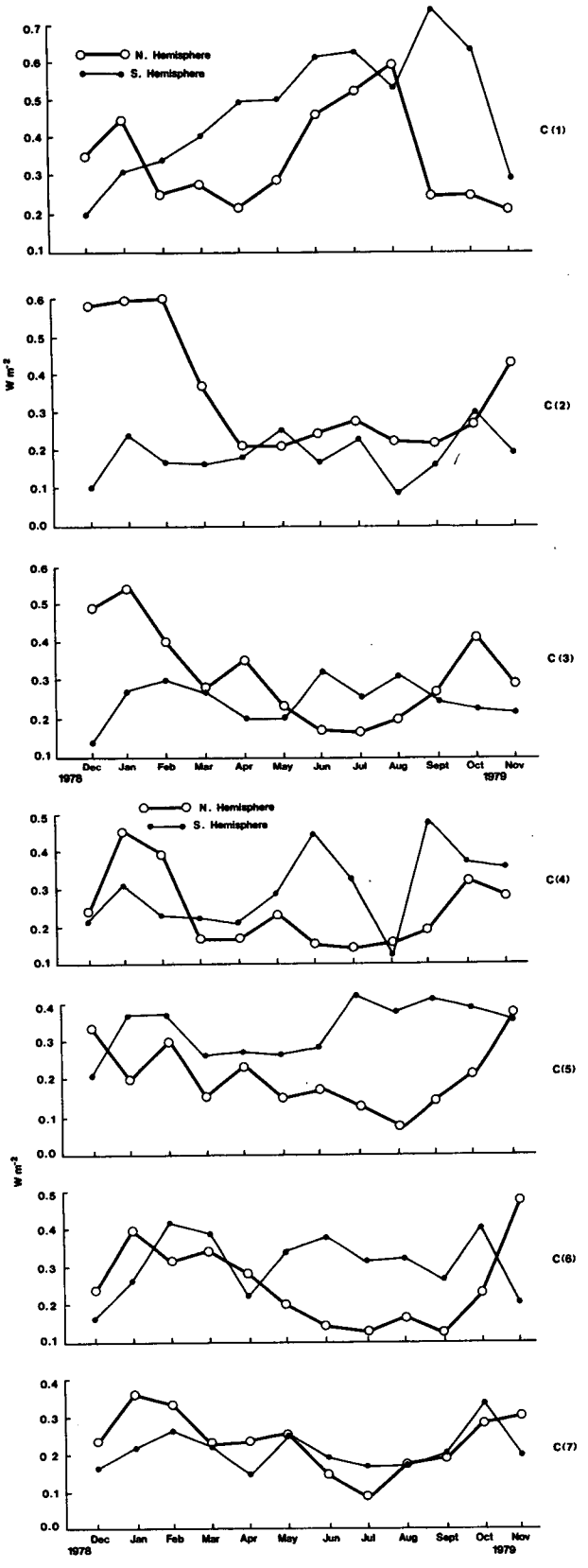

FIG. 9. As in Fig. 8 except for $C(n)$ for n = 1–7.

$K(0)$ is observed on the longer side of the period, a feature consistent with the steady zonal flow in the lower stratosphere. For waves shorter than ultralong waves, as exemplified by the large cyclone-scale wave $K(5)$, the peaks of energy shift to shorter periods. Unlike ultralong waves, the cyclone-scale waves show a noticeable difference in the spectra between the Northern and Southern hemispheres. The $K(5)$ in the Northern Hemisphere has a maximum around 20 days, and in the Southern Hemisphere around 12 and 5 days. The time spectra of $P(n)$ in Fig. 11 closely resemble those of $K(n)$ in Fig. 10, indicating a close alignment of the thermal field and the wind field in transient motions of the atmosphere.

The baroclinic conversion $C(n)$ transforms available potential energy $P(n)$ into kinetic energy $K(n)$ and is the critical linkage in the energy flow that maintains the general circulation against frictional dissipation. For the zonal mean conversion $C(0)$, the percentile ratio C_M:C_A:C_T is 77:21:2 in the Northern Hemisphere and 82:15:3 in the Southern Hemisphere. We see that for the zonal mean motion, the baroclinic conversion is mostly from the standing cells, with the remaining contribution largely from the annual migration of the cells. For eddy disturbances, as shown in Fig. 12, the

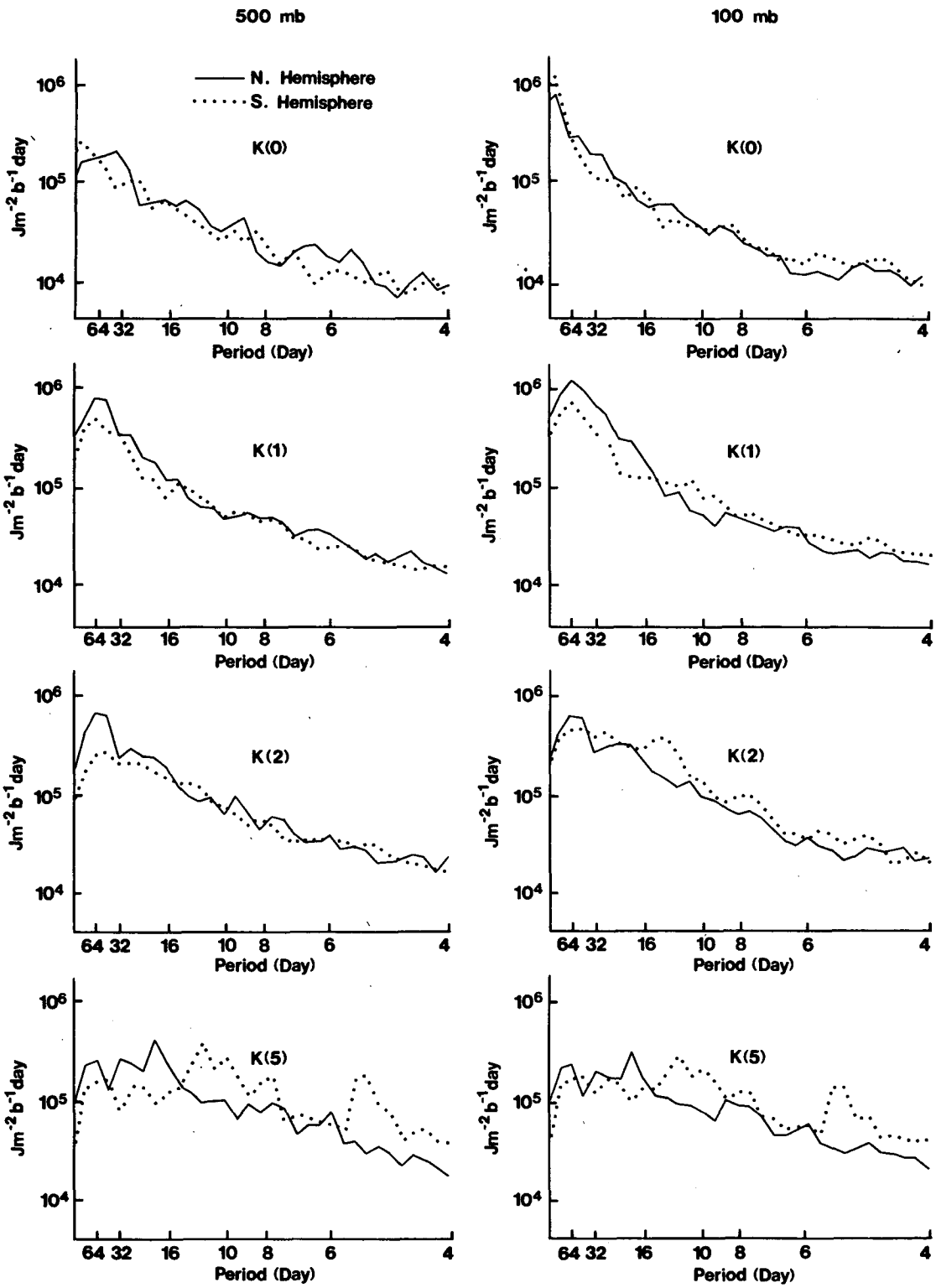

FIG. 10. Time spectra of the transient component of $K(n)$ for n = 0–5 at 500 and 100 mb in the Northern and Southern hemispheres.

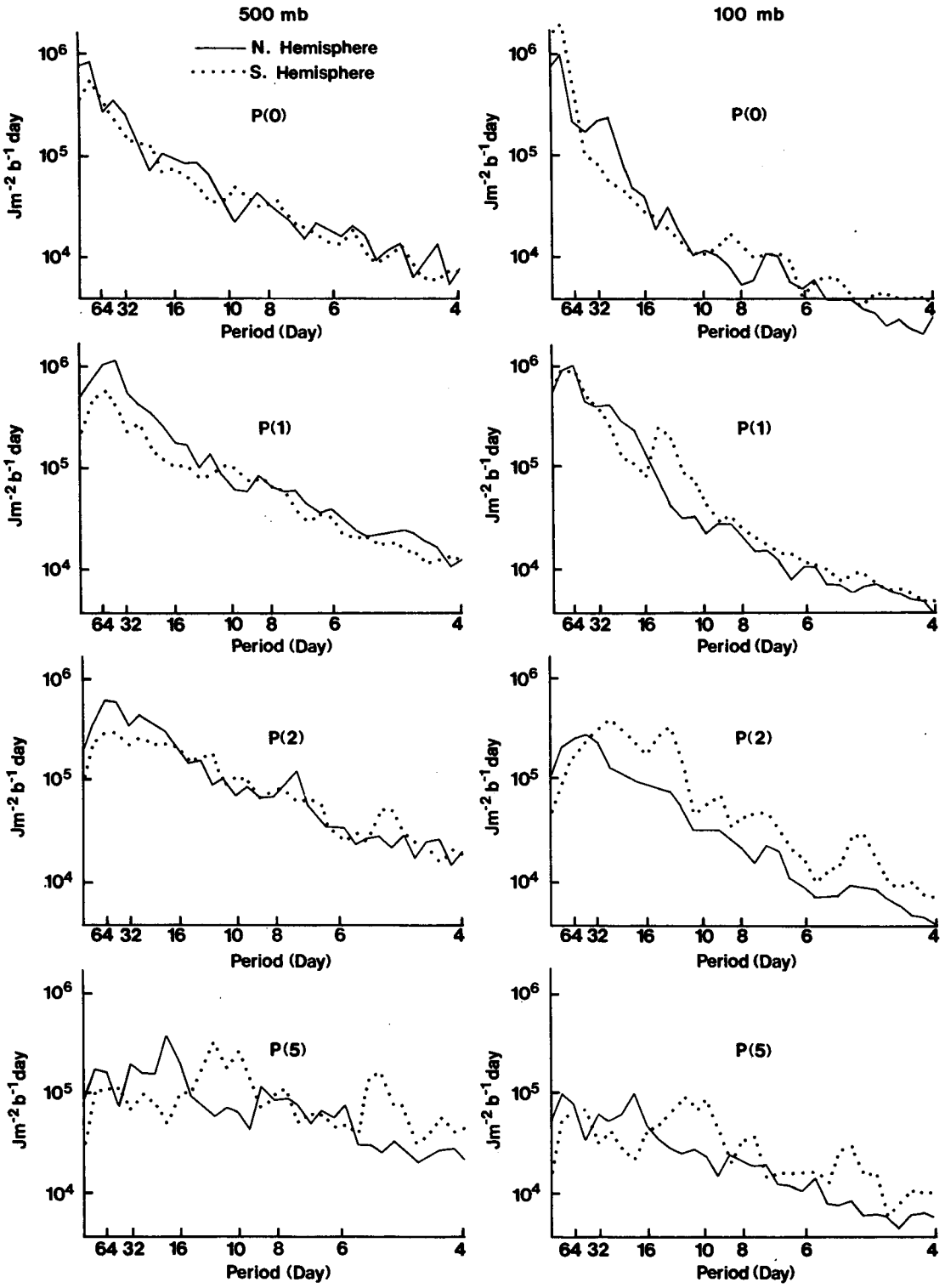

FIG. 11. As in Fig. 10 except for $P(n)$.

transient component of conversion C_T is more significant than C_M and C_A, components associated with annual mean fields and annual variations of temperature and vertical velocity at respective wavenumbers. The ultralong waves of $n = 1$, 2, and 3 in the Northern Hemisphere and $n = 1$ in the Southern Hemisphere

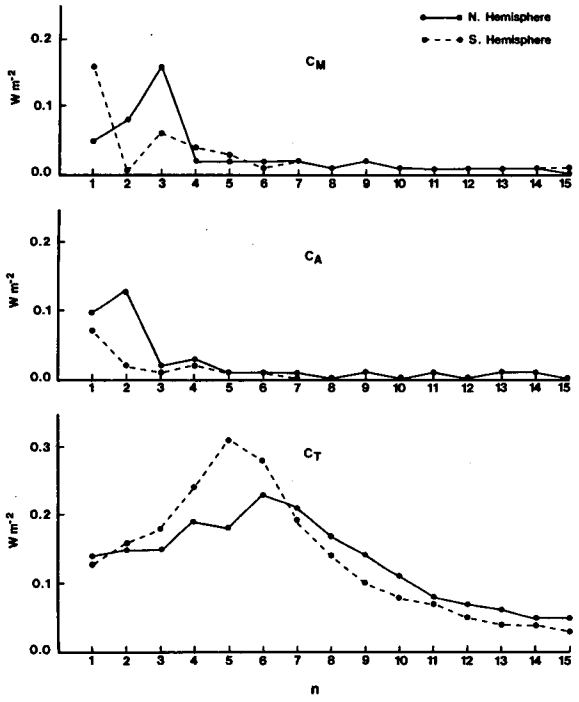

FIG. 12. Spectral distributions of the baroclinic conversion associated with the annual mean motion C_M, annual variation C_A, and transient waves C_T in the Northern and Southern hemispheres during the FGGE year.

still receive a notable contribution from C_M and C_A. However, beyond these ultralong waves, essentially all the baroclinic conversion in the cyclone-scale disturbances is associated with transient waves. The spectral distributions of C_T show a clear maximum at $n = 6$ in the Northern Hemisphere and at $n = 5$ in the Southern Hemisphere. It is noted that on large cyclone scales the transient waves are more energetically active in the Southern Hemisphere than in the Northern Hemisphere, but they become slightly less active in the shorter wave range. The difference in the hemispheric spectral distribution of baroclinic conversion $C(n)$ as shown in Fig. 5 should reflect the hemispheric differences in the activity of standing and transient waves.

Since transient waves dominate the energy conversion which takes place in the large-scale atmospheric disturbances, the baroclinic conversion by transient waves is examined with the cospectra of $B_T(t)$ and $\Omega_T(t)$ for $n = 0$–7 at 500 and 100 mb, respectively, in Figs. 13 and 14. Hemispheric differences of the cospectra are very distinctive in the midtroposphere, as shown in Fig. 13. In each hemisphere, there are also consistent but very large variations of cospectral distribution among wavenumbers. For the zonal mean wave $n = 0$ and ultralong waves $n = 1$ and 2, in which C_T is either negligibly small or only of limited importance, the conversion peaks are observed at longer periods of approximately 40–80 days. From $n = 3$ on, the cospectral peaks shift to the short periods. In the Northern Hemisphere at $n = 6$ where C_T is at the maximum, two conversion peaks are at periods of 10–20 days and 5–7 days. In the Southern Hemisphere at $n = 5$ where C_T is at the maximum, we observe two distinctive conversion peaks around 5-day and 12-day periods. It may be noted that the transient waves, which are mainly responsible for the eddy conversion of the general circulation, show characteristic but complex patterns of cospectral distributions over the frequency domain for different waves. There is a general trend that the shorter the wavelength, the shorter the corresponding period of the maximum conversion. However, due to the coexistence of various waves at each wavenumber at different latitudes, any general statement concerning the cospectral distribution would be impossible.

Comparing Fig. 13 with Fig. 10 as representative of the tropospheric situation, it is seen that the cospectra of baroclinic conversions are not as smoothly distributed over the period as those of the energy level. The discrepancy between the cospectra and power spectra may be related to the activities of nonlinear wave–wave and wave–mean interactions of kinetic energy. For example, Kung and Baker (1986a,b) identified the importance of nonlinear transfers for winter Northern Hemisphere blocking in the maintenance of kinetic energy at $n = 1$ and 2. This may be identified in part in Fig. 13 as the sharp drop of cospectra at these wavenumbers at approximately 10–20 days.

Figure 14 shows that transient waves of cyclone scale are not energetically active at the 100 mb level. In the Northern Hemisphere, significant negative conversion (destruction of kinetic energy) is indicated in the slow-moving ultralong waves and large cyclone-scale waves. These are consistent with the prevailing view that no source of energy for eddy motions appears to be present in situ in the lower stratosphere (e.g., Newell et al., 1970; Oort, 1964). It is noted here, however, that the zonal mean motion and $n = 1$ of the Northern Hemisphere and $n = 1$ and 2 of the Southern Hemisphere show a significant positive conversion at the low-frequency side. In fact, there is a similarity between the 100 and 500 mb patterns of the cospectral distribution of $n = 1$ and 2 in the Southern Hemisphere. It may be seen that the slow-moving tropospheric ultralong waves of the Southern Hemisphere extend into the lower stratosphere.

6. Concluding remarks

A basic energetics description in the zonal wavenumber domain is offered with the GFDL FGGE analysis data for the entire FGGE year. The global energy balance and those of the Northern and Southern hemispheres show a reasonable agreement in the pattern and magnitude of energy transformations, although the zonal mean field of the circulation is much stronger in

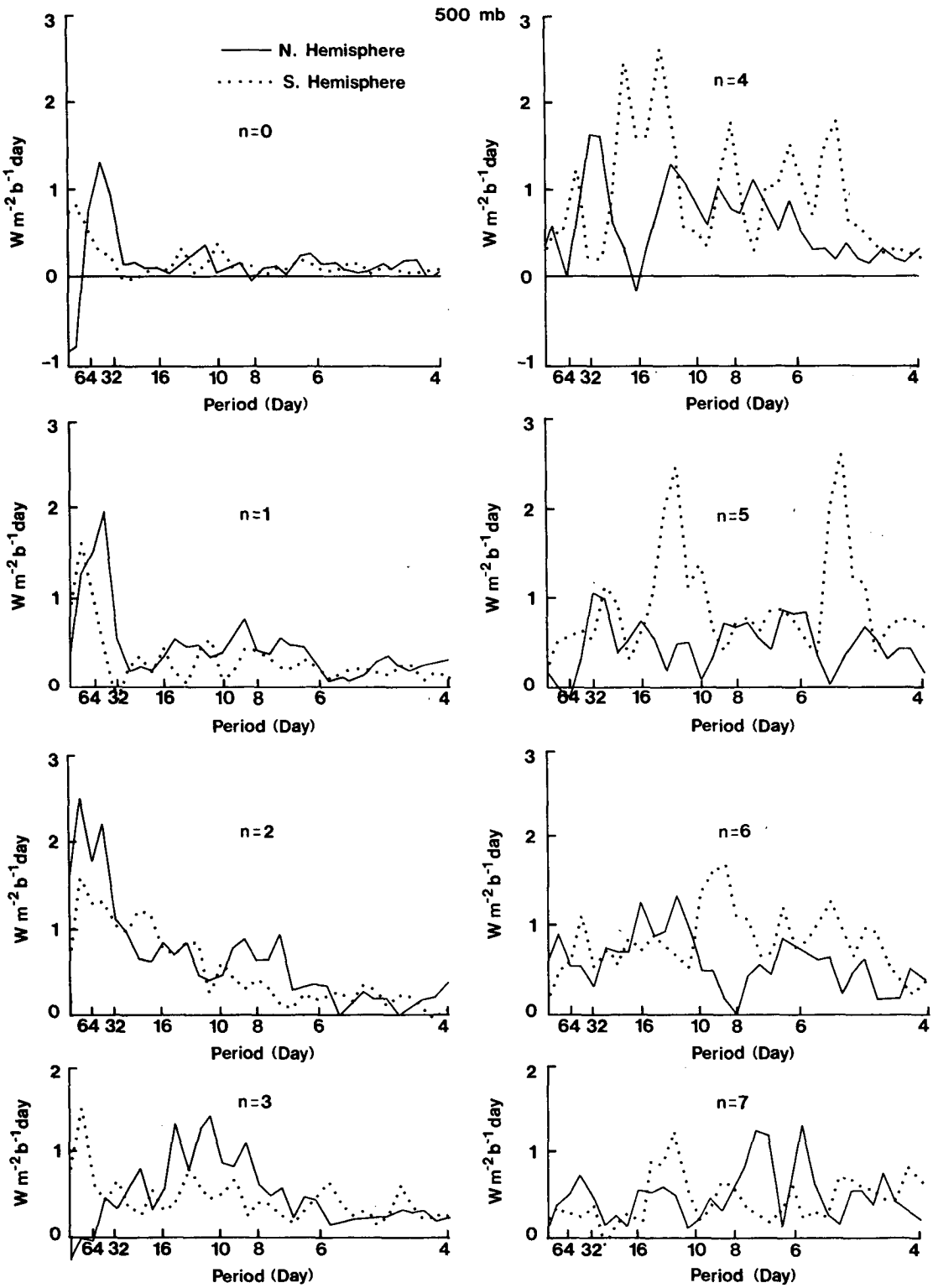

FIG. 13. Cospectral distributions of transient components of $C(n)$ for n = 0–7 in the Northern and Southern hemispheres at 500 mb.

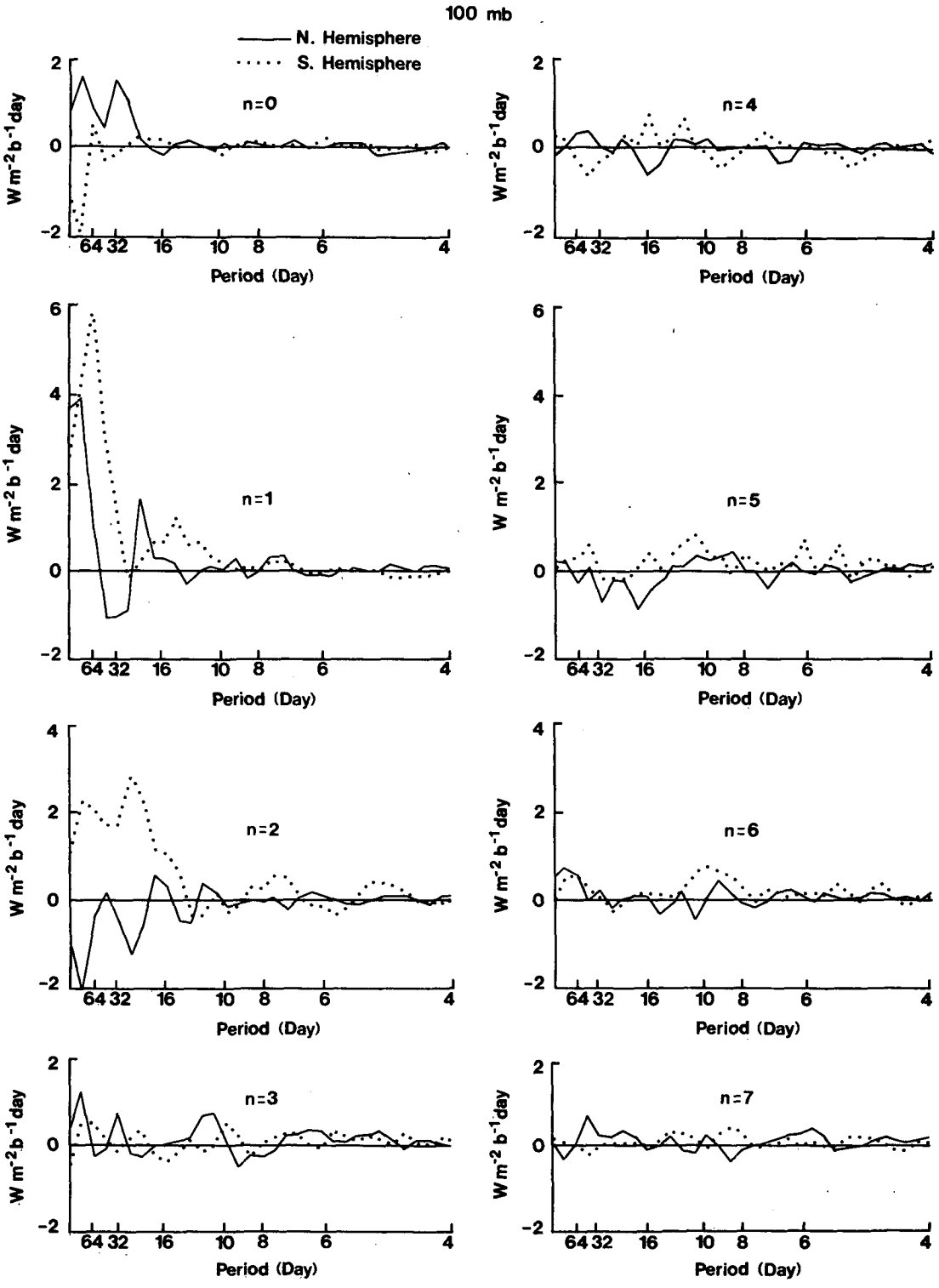

FIG. 14. As in Fig. 13 except at 100 mb.

the Southern Hemisphere than in the Northern Hemisphere. However, examination of the energy flow in the wavenumber domain reveals a marked contrast between the two hemispheres in the spectral distribution of energy and energy transformations. The differences are most pronounced for ultralong waves and large cyclone-scale waves, but the differences in the short-wave range are also noticeable. The annual vari-

ations of energy and energy transformations are large, and there are also pronounced differences in the seasonal variations between the Northern and Southern hemispheres. Although these differences are masked when the energy variables are integrated globally, they are important if energetics analyses are to be performed with reference to specific synoptic systems or model forecasts.

With the one-year time series of energy variables, time spectra of transient waves are examined with reference to kinetic energy, available potential energy and baroclinic conversion of individual wavenumbers for periods of 2–128 days. The time spectra are presented separately at 500 and 100 mb. The peak energy intensity of ultralong waves is observed around 30–60 days. The peak density shifts to shorter periods for cyclone-scale waves, with different spectral distributions for the Northern and Southern hemispheres.

On the cyclone scale almost the entire baroclinic conversion is supported by transient waves, whereas an appreciable conversion in the ultralong waves is associated with the annual mean motion and annual variations. For the ultralong waves the baroclinic conversion by transient disturbances peaks around 40–80 days, then the peak shifts to shorter periods for cyclone-scale waves. Throughout all wave ranges there is a pronounced contrast in the conversion cospectra between the Northern and Southern hemispheres. In each hemisphere a different cospectral distribution exists for each wavenumber, and the coexistence of various waves at the same wavenumber is indicated by the complex patterns of cospectral distributions. The importance of nonlinear interactions at different wavenumbers for different periods can be inferred through a comparison of kinetic energy spectra and conversion cospectra.

A three-dimensional normal mode energetics analysis was performed with the same database to describe the energy flow in the wavenumber–vertical mode domain and energy conversions between the barotropic and baroclinic components. The results will be reported in a separate paper.

Acknowledgments. The author is indebted to H. Tanaka for his assistance in the computational analysis, and to V. F. Peters and G. Vickers for their technical assistance. He is also grateful to Dr. R. D. Rosen and anonymous reviewers who provided thorough, constructive reviews in the revision of the original manuscript.

This research was jointly supported by the National Oceanic and Atmospheric Administration and the National Science Foundation under NOAA Grant NA86AA-D-AC114 and NSF Grant ATM-8410487.

REFERENCES

Arpe, K., C. Brankovic, E. Oriol and P. Speth, 1986: Variability in time and space of energetics from a long series of atmospheric data produced by ECMWF. *Beitr. Phys. Atmos.*, **59**, 321–355.

Chen, T.-C., and Y.-H. Lee, 1985: A comparison study of spectral energetics analysis using various FGGE IIIb data. *Proc. on First National Workshop on the Global Weather Experiment*, 2, 247–266. [Available from the Board on Atmospheric Sciences and Climate, 2101 Constitution Ave., Washington, DC 20418.]

Holopainen, E. O., and K. Eerola, 1979: A diagnostic study of the long-term balance of kinetic energy for atmospheric large-scale motion over the British Isles. *Quart. J. Roy. Meteor. Soc.*, **105**, 849–858.

Kao, S.-K., 1968: Governing equations and spectra for atmospheric motion and transport in frequency, wavenumber domain. *J. Atmos. Sci.*, **25**, 32–88.

Kung, E. C., 1977: Energy sources in middle-latitude synoptic-scale disturbances. *J. Atmos. Sci.*, **34**, 1352–1365.

——, and H. Tanaka, 1983: Energetics analysis of the global circulation during the special observation periods of FGGE. *J. Atmos. Sci.*, **40**, 2575–2592.

——, and ——, 1984: Spectral characteristics and meridional variations of energy transformations during the first and second special observation periods of FGGE. *J. Atmos. Sci.*, **41**, 1836–1849.

——, and W. E. Baker, 1986a: Comparative energetics of the observed and simulated global circulation during the special observing periods of FGGE. *Quart. J. Roy. Meteor. Soc.*, **112**, 593–611.

——, and ——, 1986b: Spectral energetics of the observed and simulated Northern Hemisphere general circulation during blocking periods. *J. Atmos. Sci.*, **43**, 2792–2812.

Lambert, S. J., 1986: A study of the eddy kinetic energy of the Southern Hemisphere during January and July with emphasis on the FGGE year. *Tellus*, **38A**, 429–438.

Lorenc, A. C., and R. Swinbank, 1984: On the accuracy of general circulation statistics calculated from FGGE data—a comparison of results from two sets of analyses. *Quart. J. Roy. Meteor. Soc.*, **110**, 915–942.

Lorenz, E. N., 1955: Available potential energy and the maintenance of the general circulation. *Tellus*, **7**, 157–167.

McIntyre, M. E., 1980: An introduction to the generalized Lagrangian-mean description of wave, mean-flow interaction. *Pure Appl. Geophys.*, **118**, 152–176.

Miyakoda, K., J. Sheldon and J. Sirutis, 1982: Four-dimensional analysis experiment during the GATE period. Part II. *J. Atmos. Sci.*, **39**, 486–506.

Newell, R. E., D. G. Vincent, T. G. Dopplick, D. Ferruzza and J. W. Kidson, 1970: The energy balance of the global atmosphere. *The Global Circulation of the Atmosphere*, G. S. Corby, Ed., Roy. Meteor. Soc., 42–90.

Oort, A. H., 1964: On the energetics of the mean and eddy circulation in the lower stratosphere. *Tellus*, **16**, 309–327.

——, and J. P. Peixoto, 1983: Global angular momentum and energy balance requirement from observations. *Advances in Geophysics*, Vol. 25, Academic Press, 355–490.

Plumb, R. A., 1983: A new look at the energy cycle. *J. Atmos. Sci.*, **40**, 1669–1688.

Rosen, R. D., and D. A. Salstein, 1980: A comparison between circulation statistics computed from conventional data and NMC Hough analyses. *Mon. Wea. Rev.*, **108**, 1226–1247.

——, ——, J. P. Peixoto, A. H. Oort and N.-C. Lau, 1985: Circulation statistics derived from level IIIb and station-based analyses during FGGE. *Mon. Wea. Rev.*, **113**, 65–88.

Saltzman, B., 1957: Equations governing the energetics of the larger scales of atmospheric turbulence in the domain of wavenumber. *J. Meteor.*, **14**, 513–523.

——, 1970: Large-scale atmospheric energetics in the wavenumber domain. *Rev. Geophys. Space Phys.*, **8**, 289–302.

Tanaka, H., E. C. Kung and W. E. Baker, 1986: Energetics analysis of the observed and simulated general circulation using three-dimensional normal mode expansion. *Tellus*, **38A**, 412–428.

Wiin-Nielsen, A., 1968: On the intensity of the general circulation of the atmosphere. *Rev. Geophys.*, **6**, 559–579.